Propulsion options for very low Earth orbit microsatellites

Propulsion Options for Very Low Earth Orbit Microsatellites

Mirko Leomanni[1], Andrea Garulli, Antonio Giannitrapani

Dipartimento di Ingegneria dell'Informazione e Scienze Matematiche
Università di Siena, Siena, Italy

Fabrizio Scortecci

Aerospazio Tenologie
Rapolano Terme, Siena, Italy

Abstract

The growing competitiveness in the commercial space market has raised the interest in operating small spacecraft at very low altitudes. To make this feasible, the space industry has started developing propulsion options tailored specifically to these platforms. This paper presents a review of emerging micropropulsion technologies and evaluates their applicability to microsatellite missions in the altitude range $250 - 500$ km. The results of the proposed analysis are demonstrated on two different remote sensing applications.

Keywords: Space Propulsion, Microsatellite, Low Earth Orbit, Station-Keeping

1. Introduction

In the last years, major satellite manufacturers have presented development programs for small multimission platforms, with the objective of delivering low-cost communications and Earth observation (EO) data, see, e.g., [1, 2, 3, 4, 5]. Most of these platform are designed to operate on a Low Earth Orbit (LEO), in order to contain the mission cost. In fact, the size and power consumption of optical and radar instruments scale with the orbital altitude, for a given instrument performance. Thus, a low operational altitude opens up the possibility

Email addresses: leomanni@diism.unisi.it (Mirko Leomanni), garulli@diism.unisi.it (Andrea Garulli), giannitrapani@diism.unisi.it (Antonio Giannitrapani), fscortecci@aerospazio.com (Fabrizio Scortecci)
[1]Corresponding author

of embarking high-performance payloads on board small and cheap commercial satellites.

The potential to further reduce the cost of these missions has raised the interest in operating microsatellites in orbits with an altitude below the conventional LEO range. These are commonly referred to as very low Earth orbits (VLEO), and feature an altitude between 250 km and 500 km. A number of recent studies have shown the benefits of this approach in terms of performance and cost [6, 7, 8, 9, 10]. Very low Earth orbits may also represent an effective measure to prevent space debris proliferation, due to the low debris impact probability at altitudes below 500 km [11]. On the other hand, the large atmospheric drag forces present at these altitudes can result in a severe perturbation of the orbital geometry or even a rapid decay of the orbit, unless a suitable station-keeping program is adopted. For instance, the 6 kg Dove-1 spacecraft developed by Planet Labs [12] was released in a 250 km orbit and reentered the atmosphere after 6 days.

Miniaturized chemical and electric propulsion (EP) systems represent viable options for station-keeping of microsatellites. Potential technologies include cold gas, resistojet, monopropellant, electrostatic and electromagnetic thrusters [13, 14, 15, 16, 17]. Due to the microsatellite form factor, the integration of a propulsion system is subject to stringent mass, volume and power constraints [18]. Hence, the propulsion system design must be carefully evaluated, especially for missions involving drag compensation [19, 20, 21].

Motivated by the challenges outlined above, this paper presents a review of propulsion options suitable for VLEO microsatellites. The different options are evaluated and compared for spacecraft in the $10 - 100$ kg class and mission altitudes in the $250 - 500$ km range. The most significant features of the considered technologies (deliverable thrust, specific impulse, power, lifetime, propellant type) are taken into account. The proposed analysis is demonstrated on two EO case studies involving different satellite and propulsion architectures.

The rest of the paper is organized as follows. Section 2 gives an overview on small satellite VLEO missions and introduces the mathematical models used in the following analysis. The main features of existing micropropulsion options are summarized in Section 3. These are compared in Section 4, by means of

parametric studies in which the requirements of the considered missions are taken into account. Case study applications are discussed in Section 5, and some final considerations are outlined in Section 6.

2. VLEO microsatellite missions

The ability to provide low cost, independent access to LEO for small satellites is currently seen as a strategic asset by several national and international organizations, see, e.g., the ALTAIR project within the Horizon 2020 framework [22]. The feasibility of operating small commercial spacecraft in VLEO is investigated in a number of recent studies, see, e.g., [9, 19, 23]. The following benefits are commonly acknowledged:

- Increased payload mass to orbit;
- Improved optical resolution and radiometric performance;
- Better compliance with space debris mitigation policies;
- Improved responsiveness and reduced mission cost.

Some representative examples are reported below to illustrate these points.

The payload mass which can be delivered to orbit by two dedicated small satellite launchers (Electron rocket under development at Rocket Lab [24], and air-launched Pegasus rocket developed by Orbital ATK [25]) is reported in Fig. 1. It can be seen that lowering the orbital altitude, from e.g., 800 km to 400 km, allows one to increase the payload mass delivered to orbit by up to 45%. Given that the ground sampling distance scales linearly with the altitude h and that the radiometric power density is proportional to $1/h^2$, this also improves the performance of optical and radar instruments, so that smaller instruments can be used to meet a given performance requirement. Since the spatial density of debris objects at altitudes below 500 km is at least ten times lower than that found at an orbital altitude of 800 km [26], one has a much smaller debris impact probability. Moreover, the aerodynamic drag forces present at low altitudes ensure an end-of-life deorbit time which is well below the 25-year IADC guideline [27]. Based on these considerations, the cost analysis presented in [10] for EO missions shows that VLEO microsatellites can significantly reduce the mission

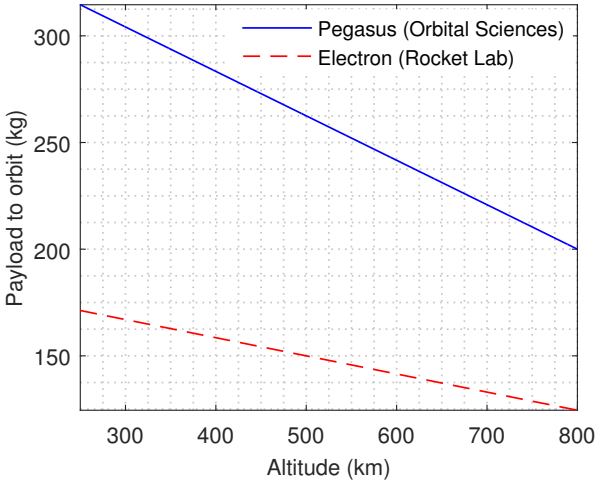

Figure 1: Launcher payload to LEO.

cost with respect to larger spacecraft flown at higher altitudes, for a fixed ground resolution and coverage performance (although a full account of the orbital decay due to drag and of the propulsion system cost is not given). The same conclusion is reached in [7] for spacecraft exploiting EP to counteract the drag force.

On the other hand, the integration of a propulsion system on board spacecraft with severe mass, volume and power limitations poses important technological and operational challenges. These are addressed in the following for the satellite missions under consideration.

2.1. Mission characteristics

Very low Earth orbits are particularly useful for EO missions [10, 19]. The following assumptions are commonly made for these missions: (i) the satellite is released in a near-circular, Sun-synchronous orbit; (ii) a frozen orbit configuration is adopted, which nullifies the perturbation of the orbital eccentricity and argument of perigee due to the Earth oblateness [28].

In this paper, the orbit altitude is treated as a free parameter taking values in the interval $250-500$ km. The effect of minor perturbations on the orbital inclination is not considered (the resulting ground-track shift can be counteracted with a negligible fuel consumption by introducing a small offset in the reference semi-major axis, to be tracked by the orbit control system [29]). The spacecraft

Table 1: Microsatellite parameters

Configuration	Mass m (kg)	Side-length l (m)	Power p (W)
C1	100	0.65	100
C2	10	0.25	15

bus layout is modeled as a cube. Two microsatellite configurations are considered, based on upper and lower bounds on the launch mass m, bus side-length l, and nominal power p generated by the solar panels. The values selected for these parameters, reported in Table 1, are consistent with the characteristics of existing platforms with body-mounted solar panels (see, e.g., the PROBA-V bus [30]). The drag coefficient is fixed to $C_d = 2.2$ for the two configurations.

The NRLMSISE-00 atmospheric model [31] is adopted to describe the lower thermosphere. The solar flux and magnetic indices are set respectively to $F10.7 = 220$ and $A_p = 40$ for a high solar and geomagnetic activity (denoted by HA), and to $F10.7 = 75$ and $A_p = 5$ for a low one (denoted by LA). The magnitude f_d of the aerodynamic drag force is modeled by the well known equation

$$f_d = \frac{C_d}{2}\, l^2\, \rho\, v^2, \tag{1}$$

where ρ indicates the average atmospheric density and v is the tangential velocity of the spacecraft. The evolution of the orbit semi-major axis a, due to perturbations, is modeled by the differential equation [32]

$$\dot{a} = 2\sqrt{\frac{a^3}{\mu}}\,\frac{u - f_d}{m}, \tag{2}$$

where u is the thrust delivered by the propulsion system and μ is the standard gravitational parameter of the Earth. Equation (2) is used with $u = 0$ to determine the orbital decay time for the parameter combinations in Table 1. The results are reported in Fig. 2 for the C1/C2 configurations and the LA/HA profiles. It can be seen that the lifetime of an uncontrolled spacecraft will not exceed one year for initial altitudes below 350 km. Also notice that smaller satellites (i.e., close to the configuration C2 in Table 1) tend to decay faster, since the ratio l^2/m is actually bigger for these platforms.

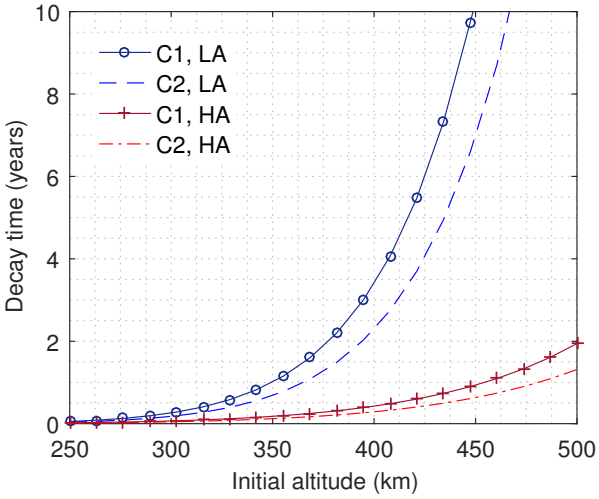

Figure 2: Orbital decay time.

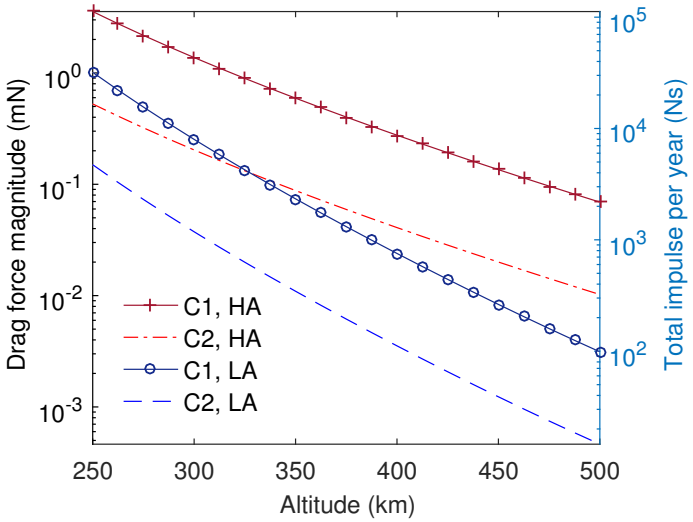

Figure 3: Drag force magnitude (y-axis on the left) and total required impulse per year (y-axis on the right) in logarithmic scale.

2.2. Station-keeping requirements

Let us assume that the orbital decay due to drag must be compensated by means of a propulsion system, and that the thrust vector is aligned with the drag force. The total impulse required for drag compensation on a time interval

T, expressed in years, can be computed as

$$J = f_d \cdot 86400 \cdot 365 \cdot T. \tag{3}$$

The total impulse per year (i.e. $T = 1$) is reported in Fig. 3 for the altitude range of interest, together with the magnitude of the drag force. Clearly, the thrust and total impulse which can be delivered by the propulsion system must be greater than f_d and J, respectively.

Many space propulsion technologies constrain the engine to operate in on-off mode, so that $u(t) \in \{0, f_t\}$ in (2), where f_t is a fixed thrust level. For these technologies, the engine duty cycle $D \in [0, 1]$ must satisfy

$$D = \frac{f_d}{f_t}, \tag{4}$$

in order to generate the total impulse needed to counteract the drag force. Notice that (4) holds under the assumption that the orbital altitude is kept reasonably close to the nominal one (i.e., if f_d is approximately constant). The number of engine cycles is dictated by the duty cycle and by the desired control accuracy. In the considered application, the thruster activation frequency can be in the order of one firing per day.

2.3. Mass, volume and power constraints

The propellant mass m_P required for station-keeping is computed as

$$m_P = \frac{J}{g_0 \, \mathrm{Isp}}, \tag{5}$$

where Isp denote the engine specific impulse and $g_0 = 9.8$ m/s^2 is the standard gravity. The wet mass of the propulsion system is estimated as

$$m_{PS} = m_P + m_S, \tag{6}$$

where m_S indicates the combined mass of the thruster, the propellant storage and supply system (dry), the power conditioning and distribution system, and the energy storage system (if present). The propulsion system mass fraction is then given by

$$\zeta = \frac{m_{PS}}{m}, \tag{7}$$

where the satellite launch mass m is fixed as in Table 1. Feasible values of ζ are usually below 0.4 [19].

Equation (5) can also be used to compute the volume V of the stored propellant, according to

$$V_P = \frac{m_P}{\rho_P}, \tag{8}$$

where ρ_P is the propellant density. The propulsion system volume is defined as

$$V_{PS} = V_P + V_S, \tag{9}$$

where V_S is the additional volume dictated by the propulsion technology (thruster, propellant supply system, power conditioning and distribution system, energy storage system). The volume fraction is then

$$\gamma = \frac{V_{PS}}{l^3}, \tag{10}$$

where l^3 denote the spacecraft bus volume. Feasible values of γ are typically below 0.3.

The power available on average on board the spacecraft is modeled as

$$p_A = \beta\, p, \tag{11}$$

where $0.5 \leq \beta \leq 1$ denotes the fraction of the orbital period in which the solar panels are exposed to the Sun and p is given in Table 1. The average power consumption of the propulsion system is estimated as

$$p_S = D\, p_I = D\, k\, f_t = k\, f_d, \tag{12}$$

where p_I denotes the instantaneous power consumption when the thruster is firing and k is the power-to-thrust ratio of the engine. Power constraints are taken into account by defining the average power fraction

$$\eta = \frac{p_S}{p_A}. \tag{13}$$

Feasible values of η are usually below 0.3 [19]. Finally, notice that p_I in (12) may be greater than p_A in (11). Indeed, for spacecraft equipped with an energy storage unit, p_I can be even larger than p. For example, the NASA iSat mission will demonstrate a 200 W Hall thruster on board a 12U, 60 W powered bus [33].

In the following, it is assumed that the mass, volume and power fractions must satisfy $\zeta \leq 0.4$, $\gamma \leq 0.3$ and $\eta \leq 0.3$, respectively. A detailed study of these requirements, for the propulsion technologies described in the next section, will be presented in Section 4.

3. Micropropulsion options

Miniaturized chemical and electric propulsion systems represent viable options for application to microsatellites. The main features of these technologies and the specifications of some engine models are summarized in this section.

3.1. Cold gas thrusters

Cold gas thrusters (CGT) consist essentially of a valve and a nozzle. They produce thrust by releasing the gas contained in a pressurized tank, so that no gas heating takes place. In principle, any gas can be used as propellant. However, mostly nitrogen, helium and butane are used in practice, because these gases are highly inert and have a reasonably low molecular mass. CGT are among the simplest type of propulsion that can be installed on a spacecraft. They are relatively lightweight, require a small amount of power and have a strong flight heritage. Typically, the combined mass of the thrusters and the propellant supply system is well below 2 kg and the power consumption is less than 10 W (valve activation).

A major drawback of this technology is the very low specific impulse and therefore the low fuel efficiency, which restricts its applicability to missions with relatively low total impulse requirements. Another shortcoming concerns the need of a pressurized propellant (for CGT fed by nitrogen and helium), since current regulations do not allow for the integration of high-pressure tanks on

Table 2: Characteristics of cold gas thrusters

						
Manufacturer	Moog	Moog	Marotta	Selex ES	MicroSpace	Vacco
Model	58X125A	58E143 58E146	Micro Thruster	Micro Thruster	MEMS	MiPS
Propellant	N_2	N_2	N_2	N_2	N_2	Butane
Thrust (mN)	4.4	16-40	50-2360	0.001-0.5	0.1-10	53
Mass (g)	9	40	< 70	300	300 (dry) Self-cont.	453 (dry) Self-cont.
Power (W)	<10	<10	<1	<1	<2	<1
Isp (s)	65	>60	65	>60	50	>60
Response (ms)	2.5	2.5	5	<100	2	<10
Min. Ibit (mN·s)			<44	<0.001	0.002	0.55
Tot. cycles	$>1.5{\cdot}10^4$	$5{\cdot}10^5$		$5{\cdot}10^8$		$8{\cdot}10^4$
Status	Flight qual. (SAFER)	Flight qual. (CHAMP)	Flight qual. (ST-5)	Flight qual. (GAIA)	Flight qual. (AlmaSat)	Flight qual. (MEPSI)

board very small satellites that are typically launched as piggyback payloads (see, e.g., C2 in Table 1). The specifications of some nitrogen CGT models are reported in Table 2, where Isp denotes the thruster specific impulse. [34, 35].

3.2. Resistojet thrusters

The working principle of resistojet thrusters is similar to that of CGT. In addition, the propellant is heated by an electrical resistance to improve the fuel efficiency, at the price of an increased power consumption. The latter can be as high as 100 W, with a typical value of about 30 W at $20-40$ mN thrust. Hence, some resistojet models may not be compatible with very small satellites, unless a suitable energy storage unit is adopted. The lifetime of this type of actuator is strongly influenced by the number of thermal cycles which can be sustained by the resistance element. These can be in excess of 10.000, for a total impulse capacity in the order of 10^4 Ns. The resitojet technology is compatible with both gaseous propellants, such as nitrogen and xenon, and two-phase propellants that are stored as a liquid, such as butane. In the second case, the vapour pressure is used to feed the thruster, while thruster heating ensures that no liquid-phase propellant is expelled. Butane resistojet systems are particularly well-suited for microsatellites, since they do not require high pressure tanks and regulation valves [36]. The specifications of several of resistojet models are summarized in Table 3 [37].

Table 3: Characteristics of resistojet thrusters

						
Manufacturer	SSTL	SSTL	Sitael	Mars Space	NanoSpace	Vacco
Model	Low power Resistojet	N_20 Rjet	XR-100	VHTR	MEMS	CHIPS
Propellant	Xe, Butane	N_20	Xe	Xe	N_2, He, Xe	R134a
Thrust (mN)	20-100	125	125	100-200	0.01-1	30
Mass (g)	90	1240	220	250	115	1.5U Pack. (wet)
Power (W)	15, 30, 50	100	80	>100	2	25
Isp (s)	48 (Xe) 90 (Butane)	127	63	80-100	50-75	82
Tot. imp. (N·s)	$5.6{\cdot}10^3$	$1.6{\cdot}10^5$	$4{\cdot}10^4$	$>10^4$		680
Temp. (deg)	500°	700°		1950°		
Status	Flight qual. (Proba-2)	Flight qual. (UoSat-12)	Under Develop.	Under Develop.	Flight qual. (PRISMA)	Under Develop.

3.3. Liquid monopropellant thrusters

Liquid monopropellant thrusters are chemical rocket engines that exploit the combustion of liquid propellants, consisting of fuel and oxidiser components, to produce thrust. They can be operated in blow-down mode: the propellant stored in a diaphragm tank is pushed by the pressurant through a catalyst bed and decomposes, initiating an exothermic reaction. Liquid monopropellant thrusters are simpler and more reliable than bipropellant thrusters and are restartable, in contrast to solid propellant thrusters. For these reasons, they are often preferred to other types of chemical engines in low and intermediate delta-v applications, such as those considered in this paper. Their power consumption is less than 15 W (engine preheating and valve activation), while their specific impulse lies between 220 s and 240 s, depending on the propellant type.

Hydrazine thrusters have a strong flight heritage and those delivering about 1 N of thrust can be easily integrated on board microsatellites. Due to the high toxicity and flammability of hydrazine, however, stringent safety precautions have to be taken throughout the whole process from design to launch. This adds high shipping costs and expensive filling operations to the already high cost of the propellant itself. For these reasons, green propellants such as LMP-103S and AF-M315E have been recently considered as a possible alternative to hydrazine [38, 15]. They offer a marginally increased performance and storage density at a significantly lower cost and risk. The specifications of some liquid

Table 4: Characteristics of liquid monopropellant thrusters

						
Manufacturer	Thales	Airbus DS	Aerojet Rocketdyne	ECAPS	Vacco	Busek
Model	RCT-1N	1N	GR-1	HPGP	ADN MiPS	BGT-X5
Propellant	Hydrazine	Hydrazine	AF-M315E	LMP-103S	LMP-103S AF-M315E	AF-M315E
Thrust (N)	1	1	1	1	0.1×4	0.5
Mass (g)	230	290	330	340	1800 (wet) Self-cont.	1500 (wet) Self-cont.
Power (W)	<15	<15	<12	<10	<15	<15
Isp (s)	220	220	231	235	>200	220
Tot. imp. (N·s)	$1.2{\cdot}10^5$	$1.3{\cdot}10^5$	$2.3{\cdot}10^4$	$5{\cdot}10^4$	$1.8{\cdot}10^3$	565
Min. Ibit (mN·s)		43	8	10	2	30
Tot. cycles	$3{\cdot}10^5$	$6{\cdot}10^4$	10^4	$6{\cdot}10^4$	10^6	
Status	Flight qual. (IRIDIUM)	Flight qual. (Globalstar)	Fight ready (GPIM)	Flight qual. (PRISMA)	Under Develop.	Under Develop.

monopropellant engines are reported in Table 4 [14].

3.4. Electrostatic/electromagnetic thrusters

Electrostatic and electromagnetic engines accelerate a ionized propellant to high velocity by using electrical energy, in order to produce thrust. Potential options for microsatellites include miniaturized Hall (HET) and radio-frequency (RF) ion thrusters, using gaseous propellants, as well as field emission (FEEP) and pulsed plasma thrusters (PPT), using liquid and solid propellants, respectively. Their specific impulse is in the $600-4500$ s range. Hence, their propellant consumption is by far lower than that provided by CGT, resistojet and monopropellant thrusters. As a rule of thumb, HET and RF thrusters should be preferred for applications involving 100-kg-class satellites (see, e.g., configuration C1 in Table 1), thanks to their relatively high thrust and total impulse capacity. FEEP and PPT thrusters, on the other hand, can be considered for smaller satellites or attitude control applications, due to their lower thrust, power consumption and impulse capability.

Disadvantages of these technologies include the high power consumption, the need of a complex power processing unit (PPU) and the low technological readiness level, which make their integration on board small satellites relatively challenging. Another concern for HET and RF thrusters is the requirement of a pressurized tank, usually storing xenon. To circumvent this issue, iodine propellant has been recently proposed as an alternative to xenon [39]. Iodine can be stored as a solid with very low vapour pressure, and heated when necessary to produce the gas required for thruster operation. It provides approximately the same performance as xenon but can be stored in a lower volume, and at a much lower pressure. A iodine-fed HET will soon be demonstrated by the NASA iSAT mission [33].

Concerns have also been raised on the survivability of EP systems in the LEO environment. Nevertheless, a number of studies aimed at investigating HET performance concluded that catodhes can survive in a relatively low vacuum environment (10^{-4} mbar), see, e.g., [40]. Similar conclusions have been reached in [41] for FEEP thrusters. The PPT technology is not seriously affected by viscous effects. Even if some interactions can take place, they cannot deteriorate the performance of the thruster to the point where its functional operation is

Table 5: Characteristics of electrostatic/electromagnetic thrusters

						
Manufacturer	Airbus DS	Busek	Aerospazio	Sitael	FOTEC	Mars Space
Model	RIT-μX	BIT-3	HET-70	HT-100	IFM 350 Nano	NanosatPPT
Type	RF	RF	HET	HET	FEEP	PPT
Propellant	Xe	I_2, Xe	Xe	Xe	Indium	Teflon
Thrust (mN)	0.01-2.5	0.3-1.6	3.5	6-18	0.001-0.5	0.09
Mass (g)	440	200	900	400	1000 (wet) Self-cont.	350 (wet) Self-cont.
Power/Thrust Ratio (W/mN)	30	42	22	20	80	55
Isp (s)	300-3000	1000-3500	1000	1000-1600	1500-4500	640
Tot. imp. (N·s)	$2{\cdot}10^5$	$>3.5{\cdot}10^4$	$>5{\cdot}10^4$ (goal)	$>5{\cdot}10^4$	$5{\cdot}10^3$	>190
Status	Under Develop.	Under Develop.	Under Develop.	Under Develop.	Under Develop.	Under Develop.

at risk. Finally, HET and RF thrusters have been proposed for the so-called RAM-EP technology, i.e. they may able to ingest atmospheric constituents and use them as propellant [42].

The main features of different thruster models are reported in Table 5 [37, 17, 16, 43]. It should be noted that FEEP engines can also be fed by cesium (see, for instance, the FT-150 thruster developed by SITAEL) or ionic liquid propellants, as outlined in [44]. The layout of an HET system is reported in Fig. 4, where the following components are shown: (i) the thruster unit (TU), including the accelerator stage (TA) and the cathode (TC); (ii) the propellant storage and supply system (PSSS), consisting of a gas tank (PSS), the pressure

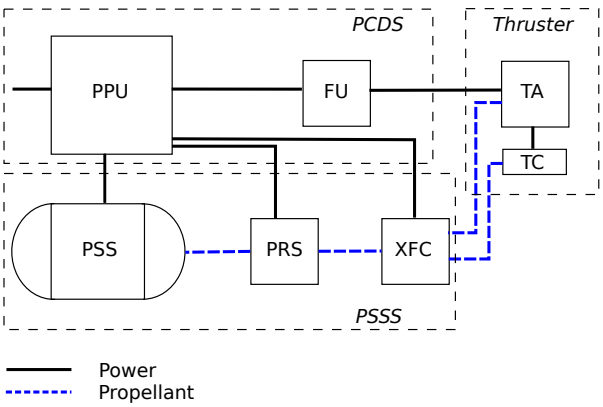

Figure 4: Layout of an HET system

regulation system (PRS) and the xenon flow controller (XFC); (iii) the power conditioning and distribution system (PCDS), including the PPU and the filter unit (FU), which is required to match the PPU output with the dynamics of the TU.

4. Propulsion system feasibility analysis

In the following, the propulsion unit mass, volume and power fractions are evaluated and compared for the technologies under consideration, based on the requirements in Section 2. Three specific impulse levels are considered:

(i) Isp=70 s, which is representative of nitrogen CGT, butane resistojets and high performance xenon resistojets (see Tables 2-3);

(ii) Isp=230 s, which is consistent with that of liquid monopropellant thrusters (see Table 4);

(iii) Isp=1000 s, which can be considered as a baseline value for electrostatic and electromagnetic thrusters (see Table 5).

The quantities m_S in (6) and V_S in (9) are estimated as in Table 6. For cold gas, resistojet and monopropellant thrusters (Isp=$70, 230$ s), the estimates are based on the characteristics of the typical micropropulsion components and the specification of the self-contained propulsion unit in Tables 2-3. PSSS, PCDS and energy storage systems designed for low-power xenon HET/RF thrusters (see Fig. 4) are considered for Isp=1000 s [45, 46]. Notice that the dry mass of the propellant tank is fixed to 15% of the propellant mass for CGT/resitojet/monopropellant thruster and to 30% (considering the features of small xenon tanks) for HET/RF systems. In a first approximation, the volume of the propulsion system is assumed coincident with the propellant volume for CGT/resistojets. For instance, the volume of the Vacco MiPS unit in Table 2 amounts to just 1% of the C2 bus volume. A pressurant volume equal to 25% of the propellant volume is taken into account for liquid monopropellant thruster, while V_S is set constant and equal to the combined volume of the PCDS, PRS and energy storage systems for HET/RF thrusters [47].

Table 6: Parameters m_S and V_S

Type	CGT, Resistojet	Monopropellant	HET/RF
C1	$m_S = 1 + 0.15\, m_P$ $V_S \approx 0$	$m_S = 2 + 0.15\, m_P$ $V_S = 0.25\, V_P$	$m_S = 10 + 0.3\, m_P$ $V_S = 0.016$
C2	$m_S = 0.5 + 0.15\, m_P$ $V_S \approx 0$	$m_S = 1 + 0.15\, m_P$ $V_S = 0.25\, V_P$	$m_S = 3 + 0.3\, m_P$ $V_S = 0.001$

The power-to-thrust ratio k in (12) is treated as a free parameter taking values in the interval $0 - 80$ W/mN, to account for the specifications of the considered technologies.

4.1. Mass fraction

Equation (7) is used to evaluate the propulsion system mass fraction for the different mission scenarios and propulsion architectures. Some representative level curves of the function ζ, which meet the constraints in Section 2.3, are depicted in Fig. 5 for the altitude range of interest and a mission design life

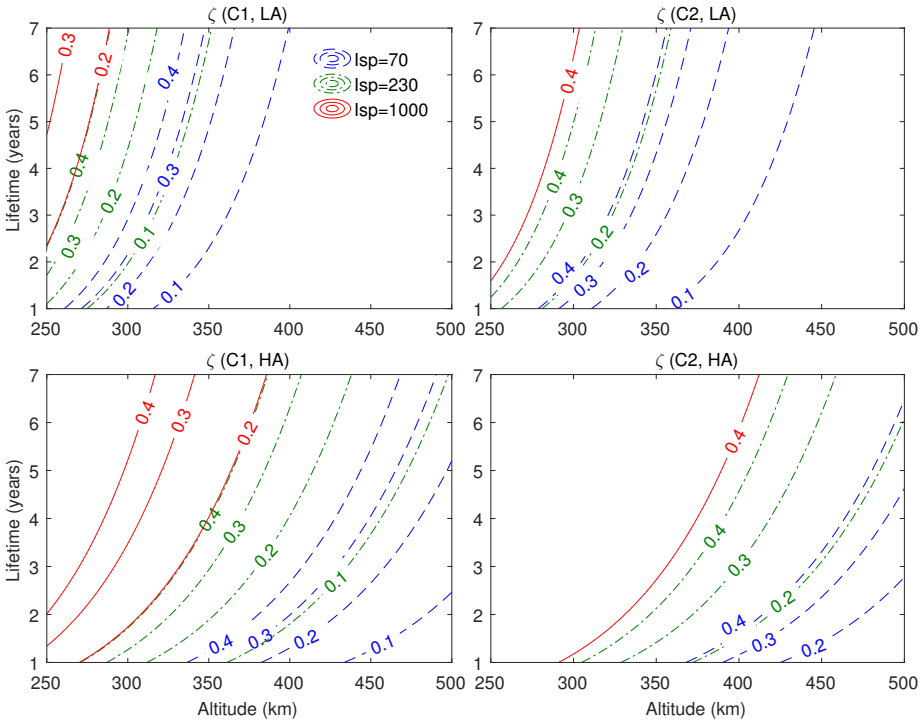

Figure 5: Propulsion system mass fraction ζ (level curves).

between $T = 1$ and $T = 7$ years. Clearly, ζ is a function which increases with the mission lifetime and decreases with the orbital altitude. Also, notice that a lower bound on ζ is imposed by the system mass which does not depend on the amount of stored propellant, reported in Table 6. For instance, $\zeta \geq 0.3$ for the C2 configuration equipped with HET/RF thruster.

It can be seen that HET/RF systems are advantageous for the C1 configuration at mission altitudes close to 250 km in the LA case, and below 350 km in the HA case. Monopropellant thrusters are preferable in the altitude intervals $285 - 340$ km (LA case) and $350 - 450$ km (HA case), while cold gas and resistojet thrusters can be considered for higher altitudes. For the C2 configuration, it should be noticed that HET and RF systems provide only a marginal performance improvement over monopropellant ones, due to their relatively high dry mass. Moreover, long duration missions are clearly not possible at altitudes below 300 km for satellites close to the configuration C2 in the HA scenario.

4.2. Volume fraction

The propulsion system volume fraction γ is evaluated by using Eq. (10). We consider nitrogen, butane, LMP103-S, xenon and iodine propellants, with the characteristics reported in Table 7.

Some representative level curves of the function γ are depicted in Fig. 6 for the orbital altitudes and the mission durations of interest. Different combinations of specific impulse levels and propellant types are reported, which model the characteristics of the considered technologies. These results basically confirm the performance figures seen in Section 4.1 for the different options. Besides

Table 7: Stored propellant characteristics

Propellant	Density ρ_P (kg/m^3)	Pressure (N/m^2)
Nitrogen	$0.28 \cdot 10^3$	$250 \cdot 10^5$ (gas)
Butane	$0.53 \cdot 10^3$	$3 \cdot 10^5$ (liquid)
LMP-103S	$1.24 \cdot 10^3$	$< 25 \cdot 10^5$ (liquid)
Xenon	$1.60 \cdot 10^3$	$120 \cdot 10^5$ (gas)
Iodine	$4.90 \cdot 10^3$	$< 1 \cdot 10^5$ (solid)

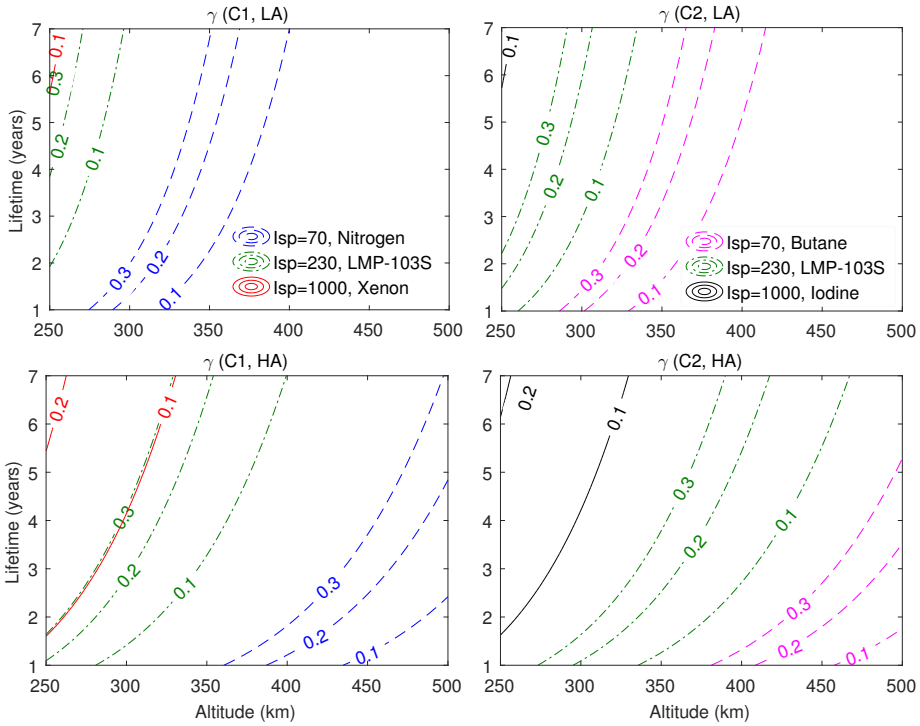

Figure 6: Propulsion system volume fraction γ (level curves).

the specific impulse, the propellant density has a key impact on the volume of the propulsion system. This is evident for RF and HET thrusters fed by xenon or iodine, for which the mass fraction in Fig. 5 is lower than the volume fraction (the density of these propellants is much greater than the overall bus density assumed in Table 1). Also notice that gaseous propellants are not considered for the C2 configuration, in compliance with current regulations on 10-kg-class satellites.

4.3. Power fraction

The propulsion system power fraction is evaluated by using (12). The results are identical for the configurations C1 and C2, since both the available power and the drag force are proportional to l^2. Some representative level curves of the function η are depicted in Fig. 7 for the power-to-thrust ratios k and the mission altitudes of interest, with $\beta = 1$. Eclipse conditions ($\beta < 1$) are taken into account by scaling the level curves by β (see (11)-(13)). Clearly, η is a function which increases with k and decreases with the altitude. Since the power-to-

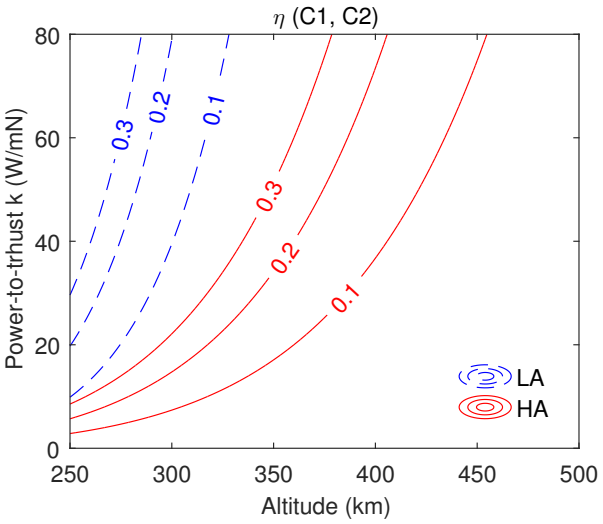

Figure 7: Propulsion system power fraction η (level curves).

thrust ratio k is dictated by the propulsion technology (see, e.g., Fig. 5), one can easily find the altitudes ranges corresponding to feasible values of of η (i.e. $\eta \leq 0.3$). In particular, it can be seen that CGT, resitojets and monopropellant technologies, whose k is typically below 2 W/mN, are largely unaffected by power constraints. HET and RF thrusters are suitable for mission altitudes down to 250 km in the LA case and above $300-350$ km (depending on β) in the HA case. PPT/FEEP thrusters meet the power constraints for altitudes above 260/280 km in the LA setting and 350/370 km in the HA setting.

5. Earth observation case studies

Propulsion candidates for a specific application can be identified by evaluating the characteristics reviewed in Section 3, against the system requirements defined in Section 2 and analyzed in Section 4. For commercial missions, the cost is usually one of the most important drivers in the selection of the propulsion system while for scientific missions the performance requirements can push the project to more complex and expensive technological solutions. A detailed assessment of operational and cost implications is complex because the information on many of the considered technologies is not homogeneous in several important factors (cost, development time, integrability) [21].

Some preliminary technical and economic considerations can still be drawn on the basis of the analysis presented in the previous section. For EO microsatellite missions, it is advisable to use a low-power propulsion system. Simultaneous thruster and payload operation should be avoided due to power, plume and thrust noise constraints. Cold gas, resitojet and monopropellant technologies are advantageous in this regard because they can be fired in short bursts, but may not be feasible for mission altitudes below 350 km (especially in the HA case, see Figs. 5-6). EP systems with a relatively low power-to-thrust ratio, such as HET and RF thrusters, can be considered for these scenarios. The applicability of self-contained EP unit based on FEEP/PPT technologies (see, e.g., Table 5) is essentially limited by power constraints for FEEP systems, due to their relatively high power-to-trust ratio, and by a very low thrust and total impulse capability for PPT (which, however, can be increased by using multiple units). In order to meet the instantaneous power demand p_I of EP thrusters, the integration of a suitable energy storage unit (i.e. batteries) may be required.

The total cost of an EO mission can be in the order of 1 M$ for a 10 kg spacecraft and of 10 M$ for a 100 kg one (see, e.g., [48]), including 30 k$ per kilogram of satellite mass due to launch costs [49]. Currently, the cost of space qualified HET and RF systems is greater than 1 M$, while that of the other technologies considered in Section 3 can be one order of magnitude lower [50]. Hence, HET and RF systems may be not economically viable for smaller spacecraft. This may change in the near future, in view of the trend towards reducing the cost of electric propulsion [20, 21]. Ground-based orbit control can be another significant cost factor, which can be minimized by adopting an autonomous station-keeping program, see, e.g., [8].

Based on these considerations, Figures 8-9 summarize the recommended application areas for the propulsion options and the satellite configurations under consideration. Two case studies are reported in the following, which fall into the two configuration classes considered in this paper.

5.1. C1 configuration, LA case

As an example of configuration C1, consider a high-resolution EO mission performed by a 100 kg microsatellite orbiting at an altitude of 275 km. The most significant mission parameters are reported in Table 8. The considered

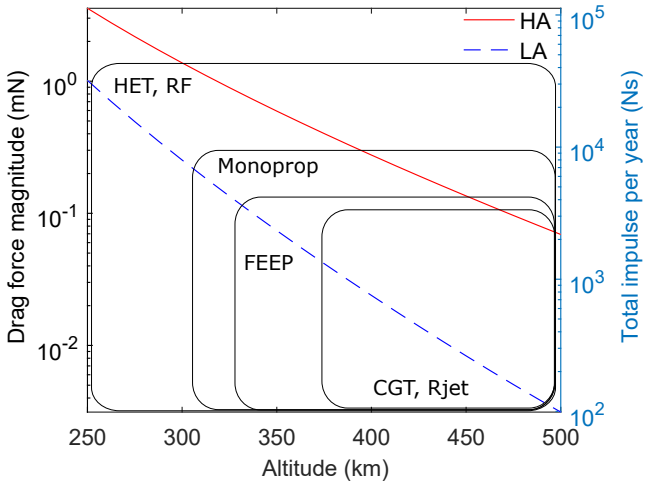

Figure 8: Application areas of micropropulsion options: C1 configuration.

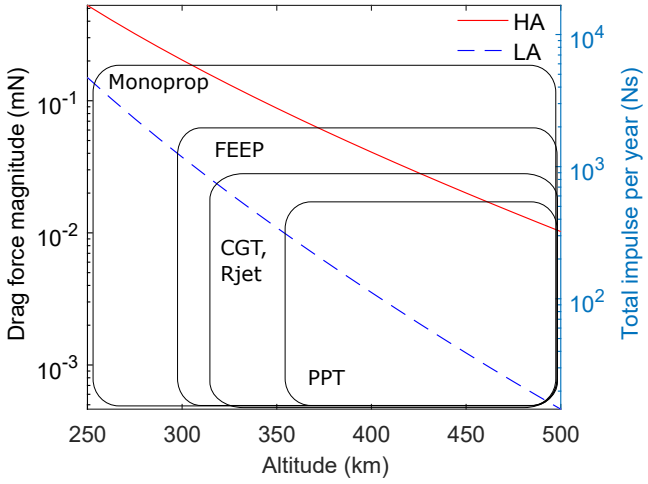

Figure 9: Application areas of micropropulsion options: C2 configuration.

payload has an aperture diameter of 0.2 m (e.g., NAOMI imager [51]), which leads to a 0.7 m ground sampling distance (GSD).

In Fig. 2, it can be seen that the orbital decay time for this mission is in the order of weeks. Hence, a propulsion system is required to achieve the target design life of 4.5 years. With the help of Fig. 8, we observe that the considered operational altitude restricts the suitable propulsion candidates to HET and RF thrusters. Among those in Table 5, we choose the HET-70 under development at Aerospazio Tecnologie [45]. The thruster is operated at its nominal thrust

Table 8: Mission parameters: C1 configuration

Orbit type:	Sun-synchronous
Orbit altitude:	275 km
Repeat period:	1 day
Activity:	LA
GSD:	0.7 m (PAN)
Design life:	4.5 years

Table 9: Propulsion system design: C1 configuration

Tot. imp. J	$7{\cdot}10^4$ Ns
Isp	1000 s
Delta-v	726 m/s
Thrust f_t	3.5 mN
Duty cycle D	0.143
No. cycles	2550
Mass fraction ζ	0.2
Volume fraction γ	0.075
Power fraction η	0.1−0.2

$f_t = 3.5$ mN and instantaneous power level $p_I = 77$ W. This is possible by using two 1 kg, 200 Wh lithium polymer batteries (see, e.g., [33]), for an overall energy storage capacity of 400 Wh. The two batteries also provide the ability to fire the engine during eclipses (see, e.g., [52]). Since the average drag force is 0.5 mN (see Fig. 8), Eq. (4) gives a duty cycle $D = 0.14$. Hence, the payload can be used for a time fraction of up to $1 - D = 0.86$. In Fig. 7 (LA case), it can be seen that the power fraction of the HET-70 system ($k = 22$ W/mN) is $\eta = 0.1$ for $\beta = 1$. This increases to $\eta = 0.2$ for $\beta = 0.5$ (see (11)-(13)). Hence, the power constraint $\eta \leq 0.3$ is met for any local mean solar time of passage (i.e., for all $\beta \in [0.5, 1]$). Figure 5 (C1, LA case) indicates that the mass of the propulsion system is 20 kg ($\zeta = 0.2$). According to (6)-(7) and Table 6, about 7.7 kg of xenon propellant are required for $\zeta = 0.2$. The propulsion system mass

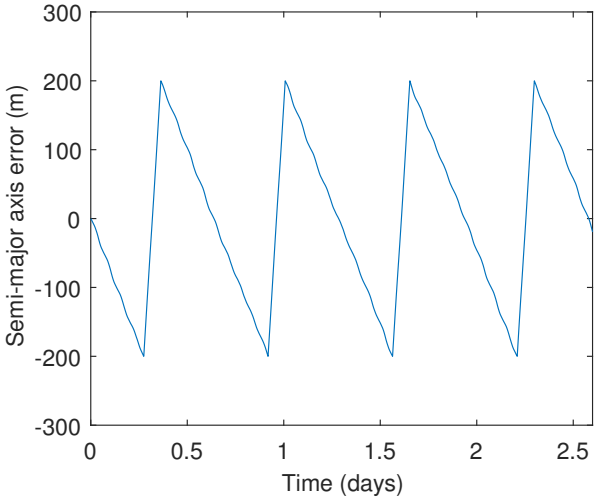

Figure 10: Semi-major axis tracking error obtained with the control law (14).

is distributed as follows: 7.7 kg of propellant, 2.3 kg for the storage tank, 7.1 kg for the PCDS and the propellant supply system, 2 kg for the batteries and 0.9 kg for the HET-70 thruster. Figure 6 shows that the propulsion system volume is less than 10% of the spacecraft bus volume ($\gamma < 0.1$). A spherical titanium tank with diameter of 21 cm is compatible with the above requirements and can be used for propellant storage.

In order to analyze in more detail the performance of the propulsion system in terms of firing maneuvers duration, number of engine cycles and power breakdown, a relay control law with hysteresis is applied to system (2). This amounts to choose

$$u(t) = \begin{cases} 3.5 \text{ mN} & \text{if} \quad a \leq a_r - h_1 \\ 0 & \text{if} \quad a \geq a_r + h_2 \\ f_p & \text{otherwise,} \end{cases} \tag{14}$$

where a_r denotes the reference semi-major axis, $h_1 > 0$ and $h_2 > 0$ define the hysteresis of the controller, and $f_p = 3.5$ mN if $a \leq a_r - h_1$ occurred more recently than $a \geq a_r + h_2$, $f_p = 0$ otherwise. More advanced strategies can be conceived to account for ground-track and maneuver location requirements, see for instance [29]. System (2),(14) has been numerically integrated for a time interval of 2.6 days, with $h_1 = h_2 = 200$ m. The error signal $a(t) - a_r$ is reported in Fig. 10. The thruster is fired once every 15.45 hours for a time

period of 2.12 hours, for an energy expenditure of 163 Wh per maneuver. The resulting duty cycle closely matches the one estimated by using (4). Based on these data, the number of engine cycles required by the station-keeping program is estimated as 2550 for the entire mission design life. The propulsion system design is summarized in Table 9.

It can be concluded that a considerable fraction of the satellite mass, volume and power is available for the payload and the other spacecraft subsystems, and that the payload operability is only marginally affected by the application of the HET system. Notice from Fig. 7 that the same conclusion cannot be reached for the HA case (in order to meet $\eta \leq 0.3$ in this case, one must have $k \leq 14$ W/mN). This is consistent to what shown in Fig. 8.

5.2. C2 configuration, HA case

As an example of configuration C2, consider a low-cost EO mission performed by a 10 kg microsatellite carrying an optical payload (aperture diameter of 0.1 m), at an altitude of 370 km. The main parameters of the mission are summarized in Table 10.

In Fig. 2, it can be seen that the orbital decay time for this mission is in the order of few months. Once again, a propulsion system is required to achieve the target design life. Figure 9 suggests the application of liquid monopropellant or FEEP thrusters. Let us consider first the HPGP monopropellant thruster developed by ECAPS (see Table 4), which is fed by a green propellant and has been flight qualified within the PRISMA mission [53]. Since the average drag force is $f_d = 0.065$ mN (see Fig. 9) and the nominal thrust level is $f_t = 1$ N, Eq. (4) gives a very small duty cycle $D = 6.5 \cdot 10^{-5}$. Hence, the payload operability is mostly unaffected by station-keeping operations. According to (2), a station-keeping maneuver must be performed once every two days to keep the orbit semi-major axis within ± 1 km from the reference. The duration of each firing is about 10 s, which is above the minimum firing time of the thruster. Power constraints (see Fig. 7) are clearly met because the power-to-thrust ratio k of the engine is smaller than 10^{-2} W/mN (see Table 4). According to Fig. 5 (C2, HA case), the mass of the propulsion system is 3 kg ($\zeta = 0.3$). About 1.7 kg of LMP103-S propellant are needed for $\zeta = 0.3$. Figure 6 shows that the propulsion system volume amounts to approximately 10% of the bus volume

Table 10: Mission parameters: C2 configuration

Orbit type:	Sun-synchronous
Orbit altitude:	370 km
Repeat period:	3 days
Activity:	HA
GSD:	2 m (PAN)
Design life:	2 years

Table 11: Propulsion system design: C2 configuration

Tot. imp. J	$4.1{\cdot}10^3$ Ns
Isp	230 s
Delta-v	452 m/s
Thrust f_t	1 N
Duty cycle D	$6.5{\cdot}10^{-5}$
No. cycles	365
Mass fraction ζ	0.3
Volume fraction γ	0.1
Power fraction η	$<9{\cdot}10^{-5}$

($\gamma = 0.1$), which leaves a considerable fraction of the latter available for the other spacecraft subsystems. The propulsion system design is summarized in Table 11.

Compared to the HPGP, the IFM 350 Nano unit under development at FOTEC (see Table 5), which is a 1 kg (wet), $10{\times}10{\times}10$ cm^3 module containing the whole system (TU, PSSS, PCDS) [16], would lead to lower volume and mass fractions. Moreover, the $5 \cdot 10^3$ Ns total impulse which can be delivered by this unit is well above the required one. On the other hand, a constant illumination of the solar panels is necessary to meet the power constraints, due to the high power-to-thrust ratio (80 W/mN) of the engine. In fact, Fig. 7 indicates that $\eta \leq 0.3$ is barely met for $\beta = 1$, and Fig. 9 shows that the considered mission altitude is at the border of the FEEP application area. Therefore, the satellite

must be operated in a dawn/dusk orbit. This last requirement can be relaxed by installing deployable solar arrays which may, however, induce more drag and increase the cost of the spacecraft.

6. Conclusions

Propulsion options suitable for station-keeping of microsatellites in very low Earth orbits have been reviewed and compared. The developed analysis and design tools enable a rapid assessment of the applicability of these technologies to missions featuring different satellite layouts, operational altitudes and design life. Applications involving remote sensing microsatellites of different size have been investigated in detail and appear to be feasible, provided that the propulsion system is carefully chosen to meet the satellite (mass, volume, power) and operational (duty cycle, lifetime) constraints. The propulsion system cost is another critical factor to be taken into account in the comparison. A detailed cost analysis will be addressed by future works, as soon as the considered technologies will reach a more defined commercial status.

Acknowledgements

The authors would like to thank the anonymous reviewers for their valuable comments and suggestions, which greatly improved the quality of the paper.

References

[1] M. Fouquet, M. Sweeting, UoSAT-12 minisatellite for high performance Earth observation at low cost, Acta Astronautica 41 (3) (1997) 173–182.

[2] G. Tyc, J. Tulip, D. Schulten, M. Krischke, M. Oxfort, The RapidEye mission design, Acta Astronautica 56 (1) (2005) 213–219.

[3] A. da Silva Curiel, L. Boland, J. Cooksley, M. Bekhti, P. Stephens, W. Sun, M. Sweeting, First results from the disaster monitoring constellation (DMC), Acta Astronautica 56 (12) (2005) 261–271.

[4] J. Bermyn, C. Dorn, PROBA spacecraft family - Small mission solutions for emerging applications, in: Small Satellites for Earth Observation: Selected Contributions, 2008, pp. 67–76.

[5] K. Murthy, M. Shearn, B. D. Smiley, A. H. Chau, J. Levine, D. Robinson, Skysat-1: very high-resolution imagery from a small satellite, in: Proc. SPIE 9241, Sensors, Systems, and Next-Generation Satellites, International Society for Optics and Photonics, 2014, XVIII, 92411E.

[6] M. Guelman, A. Kogan, Electric propulsion for remote sensing from low orbits, Journal of Guidance, Control, and Dynamics 22 (2) (1999) 313–321.

[7] D. G. Fearn, Economical remote sensing from a low altitude with continuous drag compensation, Acta Astronautica 56 (5) (2005) 555–572.

[8] A. Garulli, A. Giannitrapani, M. Leomanni, F. Scortecci, Autonomous low-Earth-orbit station-keeping with electric propulsion, Journal of Guidance, Control, and Dynamics 34 (6) (2011) 1683–1693.

[9] J. V. Llop, P. C. Roberts, Z. Hao, L. R. Tomas, V. Beauplet, Very Low Earth Orbit mission concepts for Earth observation. Benefits and challenges, in: 12th Reinventing Space Conference, London, United Kingdom, 2014.

[10] A. Shao, E. A. Koltz, J. R. Wertz, Quantifying the cost reduction potential for Earth Observation satellites, in: 12th Reinventing Space Conference, London, United Kingdom, 2014.

[11] R. Walker, C. Martin, Cost-effective and robust mitigation of space debris in Low Earth Orbit, Advances in Space Research 34 (5) (2004) 1233–1240.

[12] W. Marshall, C. Boshuizen, Planet Labs' remote sensing system, in: 27th AIAA/USU Conference on Small Satellites, Logan, United States, 2013.

[13] R. M. Myers, S. R. Oleson, F. M. Curran, S. J. Schneider, Small satellite propulsion options, in: 30th Joint Propulsion Conference, Indianapolis, United States, 1994.

[14] J. Mueller, Thruster options for microspacecraft: a review and evaluation of state-of-the-art and emerging technologies, Progress in Astronautics and Aeronautics 187 (2000) 45–138.

[15] A. S. Gohardani, J. Stanojev, A. Demair, K. Anflo, M. Persson, N. Wingborg, C. Nilsson, Green space propulsion: Opportunities and prospects, Progress in Aerospace Sciences 71 (2014) 128–149.

[16] A. Reissner, N. Buldrini, B. Seifert, T. Hrbe, P. Florin, C. Scharlemann, Introducing very high Δv capability to nanosats and cubesats, in: 34th International Electric Propulsion Conference, Hyogo-Kobe, Japan, 2015.

[17] W. Wright, P. Ferrer, Electric micropropulsion systems, Progress in Aerospace Sciences 74 (2015) 48 – 61.

[18] V. Zakirov, M. Sweeting, P. Erichsen, T. Lawrence, Specifics of small satellite propulsion: Part 1, in: 15th AIAA/USU Conference on Small Satellites, Logan, United States, 2001.

[19] N. Arcis, A. Varinois, J. M. Ruault, M. Gollor, J. Roggen, K. Ruf, Database of EPS key requirements and technical specifications for current and future missions, Tech. rep., Centre National d'Etudes Spatiales (2015).

[20] N. Arcis, EPIC Partners, EPIC 1st Workshop report, Tech. rep., Centre National d'Etudes Spatiales (2015).

[21] J. L. Reig, C. G. Sacristan, N. Arcis, K. Ruf, A. Bulit, Studies and analysis of requirements vs. application domains, Tech. rep., Centre National d'Etudes Spatiales (2015).

[22] `http://cordis.europa.eu/project/rcn/199831_en.html`, accessed: 14-07-2016.

[23] M. Leomanni, A. Garulli, A. Giannitrapani, P. Pergola, F. Petroni, F. Scortecci, SSCAM: Micro-satellite platform for Earth observation, in: 10th IAA Symposium on Small Satellites for Earth Observation, Berlin, Germany, 2015.

[24] `https://www.rocketlabusa.com`, accessed: 08-04-2016.

[25] Orbital ATK, Pegasus user guide (2015).

[26] Orbital debris quarterly news, vol. 18, No. 2, NASA, 2014.

[27] IADC space debris mitigation guidelines, Inter-Agency Space Debris Coordination Committee, 2007, revision 1.

[28] D. A. Vallado, Fundamental of Astrodynamics and Applications, 2nd Edition, Microcosm Press, El Segundo, California, 2001, chap. 11.

[29] X. Fu, M. Wu, Y. Tang, Design and maintenance of low-Earth repeat-ground-track successive-coverage orbits, Journal of Guidance, Control, and Dynamics 35 (2) (2012) 686–691.

[30] M. Francois, S. Santandrea, K. Mellab, D. Vrancken, J. Versluys, The PROBA-V mission: the space segment, International Journal of Remote Sensing 35 (7) (2014) 2548–2564.

[31] J. M. Picone, A. E. Hedin, D. P. Drob, A. C. Aikin, NRLMSISE-00 empirical model of the atmosphere: Statistical comparisons and scientific issues, Journal of Geophysical Research: Space Physics 107 (A12) (2002) SIA 15–1–SIA 15–16.

[32] R. H. Battin, An introduction to the mathematics and methods of astrodynamics, AIAA, 1999.

[33] J. W. Dankanich, K. A. Polzin, D. Calvert, H. Kamhawi, The iodine Satellite (iSAT) Hall thruster demonstration mission concept and development, in: 50th Joint Propulsion Conference, Cleveland, United States, 2014.

[34] J. Mueller, J. Ziemer, R. Hofer, R. Wirz, T. O'Donnell, A survey of microthrust propulsion options for microspacecraft and formation flying missions, in: 5th CubeSat Developers Workshop, San Luis Obispo, United States, 2008.

[35] G. Matticari, M. Materassi, G. Noci, L. Fallerini, P. Siciliano, Use of a "wide dynamic range" electronic flow regulator to increase the flexibility and versatility of electric and cold gas small propulsion systems, in: 32nd International Electric Propulsion Conference, Wiesbaden, Germany, 2011.

[36] D. Gibbon, C. Underwood, M. Sweeting, R. Amri, Cost effective propulsion systems for small satellites using butane propellant, Acta Astronautica 51 (19) (2002) 145–152.

[37] N. Arcis, A. Bulit, M. Gollor, P. Lionnet, J. C. Treuet, I. A. Gomez, Database on EP (and EP-related) technologies and TRL, Tech. rep., Centre National d'Etudes Spatiales (2015).

[38] R. L. Sackheim, R. K. Masse, Green propulsion advancement: challenging the maturity of monopropellant hydrazine, Journal of Propulsion and Power 30 (2) (2014) 265–276.

[39] J. Szabo, M. Robin, S. Paintal, B. Pote, V. Hruby, C. Freeman, Iodine propellant space propulsion, in: 33rd International Electric Propulsion Conference, Washington, United States, 2013.

[40] H. Simpson, N. Wallace, D. Fearn, M. Kelly, A summary of the QinetiQ hollow cathode development programme in support of European high power Hall effect and gridded thrusters, in: 28th International Electric Propulsion Conference, Toulouse, France, 2003.

[41] F. Ceccanti, S. Marcuccio, M. Andrenucci, FEEP thruster survivability in the LEO atomic oxygen environment, in: 27th International Electric Propulsion Conference, Pasadena, United States, 2001.

[42] L. A. Singh, M. L. Walker, A review of research in low Earth orbit propellant collection, Progress in Aerospace Sciences 75 (2015) 15–25.

[43] M. Coletti, S. Ciaralli, S. B. Gabriel, PPT development for nanosatellite applications: Experimental results, IEEE Transactions on Plasma Science 43 (1) (2015) 218–225.

[44] S. Marcuccio, N. Giusti, P. Pergola, Slit FEEP thruster performance with ionic liquid propellant, in: 49th AIAA Joint Propulsion Conference and Exhibit, San Jose, United States, 2013.

[45] F. Scortecci, Development of a low power electric propulsion system for mini-sats applications, in: Le Tecnologie Nazionali per mini e micro satelliti: Idee, Progetti e Prospettive (CIRA Workshop), Capua, Italy, 2015.

[46] M. Gollor, A. Franke, U. Schwab, W. Dechent, G. Glorieux, M. Boss, N. Wagner, J. Palencia, P. Galatini, G. Tuccio, E. Bourguignon, Power Processing Units-Activities in Europe 2015, in: 34th International Electric Propulsion Conference, Hyogo-Kobe, Japan, 2015.

[47] P. Erichsen, Performance evaluation of spacecraft propulsion systems in relation to mission impulse requirements, in: European Spacecraft Propulsion Conference, Vol. 398, 1997, pp. 189–196.

[48] M. Thoby, Myriade: CNES micro-satellite program, in: 15th AIAA/USU Conference on Small Satellites, Logan, United States, 2001.

[49] D. Koelle, R. Janovsky, Development and transportation costs of space launch systems, in: DGLR/CEAS European Air and Space Conference, Berlin, Germany, 2007.

[50] T. Lawrence, J. Sellers, J. Ward, M. Paul, Results of low-cost electric propulsion system research for small satellite application, in: 15th AIAA/USU Conference on Small Satellites, Logan, United States, 1996.

[51] P. Luquet, A. Chikouche, A. Benbouzid, J. Arnoux, E. Chinal, C. Massol, P. Rouchit, S. de Zotti, NAOMI instrument: a product line of compact & versatile cameras designed for high resolution missions in Earth observation, in: 7th International Conference on Space Optics, Toulouse, France, 2008.

[52] A. Bechi, S. Gregucci, A. Papa, P. Pergola, S. Marcuccio, Electric propulsion microsatellites in a versatile constellation for remote sensing applications, in: 10th IAA Symposium on Small Satellites for Earth Observation, Berlin, Germany, 2015.

[53] K. Anflo, R. Möllerberg, Flight demonstration of new thruster and green propellant technology on the PRISMA satellite, Acta Astronautica 65 (9) (2009) 1238–1249.

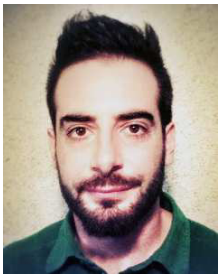

Mirko Leomanni was born in Siena, Italy, in 1983. He received the M.Sc. degree in Information Engineering in 2008, and the Ph.D. in Information Engineering and Science in 2015, both from the University of Siena. Since 2015, he is a research associate in automatic control and robotics at the University of Siena. His research interests include spacecraft dynamics and control, analysis of switching systems, optimization, and autonomous navigation.

Andrea Garulli was born in Bologna, Italy, in 1968. He received the Laurea in Electronic Engineering from the Università di Firenze in 1993, and the Ph.D. in System Engineering from the Università di Bologna in 1997. In 1996 he joined the Università di Siena, where he is currently Professor of Control Systems. Since 2015, he is the director of the Dipartimento di Ingegneria dell'Informazione e Scienze Matematiche. He has been member of the Conference Editorial Board of the IEEE Control Systems Society and Associate Editor of the IEEE Transactions on Automatic Control. He currently serves as Associate Editor for Automatica. He is author of more than 170 technical publications, co-author of the book "Homogeneous Polynomial Forms for Robustness Analysis of Uncertain Systems" (Springer, 2009) and co-editor of the books "Robustness in Identification and Control" (Springer, 1999), and "Positive Polynomials in Control" (Springer, 2005). His present research interests include system identification, robust estimation and filtering, robust control, mobile robotics, autonomous navigation and aerospace systems.

Antonio Giannitrapani was born in Salerno, Italy, in 1975. He received the Laurea degree in Information Engineering in 2000, and the Ph.D. in Control Systems Engineering in 2004, both from the University of Siena. In 2005 he joined the Dipartimento di Ingegneria dellInformazione e Scienze Matematiche of the same university, where he is currently Assistant Professor. His research interests include localization and map building for mobile robots, motion coordination of teams of autonomous agents and attitude control systems of satellites.

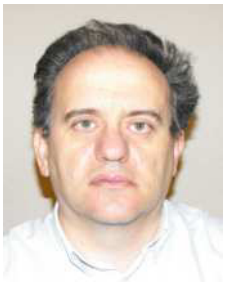

Fabrizio Scortecci received a MS in Aerospace Engineering at the Università di Pisa in 1990. Since his graduation he worked as a Researcher and then as a Project Manager in various theoretical and experimental projects related to electric satellite propulsion, aerothermodynamics and spacecraft systems. During the year 2000 he joined AEROSPAZIO Tecnologie s.r.l. working as Senior Scientist and Manager on programs related to on-orbit application of electric propulsion.